

Low-Cost, Series–Parallel-Fed 2-Bit Phased Array Antenna in Ku -Band

Lu Yin , Peng Yang , *Member, IEEE*, Tao Dong , Jun Hu , *Senior Member, IEEE*,
and Zaiping Nie , *Fellow, IEEE*

Abstract—In this letter, a low-cost, series–parallel-fed 2-bit phased array antenna for Ku -band 1-D beam scanning application is presented. The compact 2-bit element consists of a microstrip patch with $0^\circ/180^\circ$ phase states, dc bias circuits, ground, and a cascaded 90° phase shifter. Using the proposed element, a series–parallel-fed 9×8 array is fabricated and measured. Experimental results demonstrate the beam scanning capability in H-plane within the scan range of $\pm 50^\circ$, and also show high agreement compared with the simulated ones.

Index Terms—2-bit, beam scan, p-i-n diodes, phased-array antenna, reconfigurable.

I. INTRODUCTION

RECENTLY, beam scanning antennas based on electrical tuning switches have gotten a lot of interest. Antennas with switchable beams can determine the target location and then radiate the signal in the right direction to keep the wireless connection between the base station and the target as stable as possible. Especially in a limited space, multipath fading is exacerbated by the presence of multiple scatterers. As a low-cost wireless relay, this kind of antenna provides a complementary link for the communication system [1], [2]. Furthermore, studies have shown that antenna arrays with steerable beams can effectively lower the data collision rate and energy consumption of communication nodes compared with omnidirectional antennas [3], [4].

p-i-n diodes provide digitally controlled scheme for electronically beam scanning antennas. This approach has been applied in [5], [6], [7], [8], [9], [10], [11], [12], [13], and [14]. Compared with spatial-fed arrays, radiative arrays have low-profile characteristics, and various designs have been proposed. In [7], a $0^\circ/90^\circ$ miniaturized phase shifter (about $0.24 \lambda_g \times 0.13 \lambda_g$) working at 1.5 GHz was proposed. Utilizing the symmetry of the antenna element, the $0^\circ/180^\circ$ phase states can be realized, and then, a 90° digital phase shifter was cascaded to the antenna

TABLE I
COMPARISON BETWEEN THE PROPOSED ARRAY AND EXISTING LITERATURE

Ref.	[7]	[8]	[14]	[12]	Prop.
Fre. (GHz)	1.5	3.65	4.8	27	17.3
Element Size	0.5λ	0.51λ	0.6λ	0.54λ	0.46λ
Diodes Num. (Element)	4	4	10	2	4
N bit	2	2	2	1	2
Scanning Range	28°	$\pm 49^\circ$	$\pm 45^\circ$	-34° to 35°	$\pm 50^\circ$

element to achieve 2-bit phase resolution. Similarly, a 2-bit circularly polarized array operating at 3.65 GHz was presented in [8]. In [9], a C -band 4-bit composite right-/left-handed phase shifter was designed by integrating four diodes. However, due to the large size of the antenna, the beam scanning range is limited to 38° . The phase distribution of the series-fed antenna can be disturbed by the p-i-n diodes, which will change the direction of the main beam. In [10], a fixed-frequency 2-bit leaky-wave antenna was tested at 5 GHz. An S -band 2-bit element with only three p-i-n diodes was presented in [11]. In addition, utilizing the rotational symmetry of the CP antenna, 2-bit beam scanning array was also achieved in 3 [13] and 5 GHz [14]. From the foregoing, it can be seen that 2-bit radiative antennas have grown in popularity recently.

However, high-frequency antenna design becomes more challenging due to the smaller size and higher integration. At present, most of the literature focuses on the frequency band below 5 GHz, as given in Table I. Here, we propose a low-cost, series–parallel-fed 2-bit phased array antenna working at Ku -band. For 1-D beam scanning applications, such as automotive radar, the series-fed linear subarray has the advantage of higher gain, which can effectively compensate the influence of high-frequency path loss. A low-profile, compact 2-bit microstrip antenna is adopted as the phase shifter to drive the series-fed linear subarray with 0° , 90° , 180° , and 270° phase states. Finally, a 9×8 prototype based on the subarray has been fabricated and measured to verify the 1-D beam scanning property.

II. DESIGN OF 1-D SCANNING ANTENNA ARRAY

A. Compact 2-Bit Antenna Element

The basic structure of the proposed element is shown in Fig. 1, which consists of two layers of Rogers 4350B substrates ($\epsilon_r = 3.66$, $\tan \delta = 0.004$). The thicknesses of the upper and lower

Manuscript received 3 December 2022; accepted 26 December 2022. Date of publication 29 December 2022; date of current version 5 May 2023. This work was supported in part by the NSFC under Grant 62171103 and Grant 61871101; in part by the Sichuan Provincial Science and Technology Support Program under Grant 2021ZHYZ20001; and in part by the “111” project under Grant BP0719011. (Corresponding author: Peng Yang.)

Lu Yin, Peng Yang, Jun Hu, and Zaiping Nie are with the School of Electronic Science and Engineering, University of Electronic Science and Technology of China, Chengdu 611731, China (e-mail: yyinlu@163.com; yangpeng@uestc.edu.cn; hujun@uestc.edu.cn; zpnjie@uestc.edu.cn).

Tao Dong is with the State Key Laboratory of Space-Ground Integrated Information Technology, Beijing Institute of Satellite Information Engineering, Beijing 100095, China (e-mail: dongtaoandy@163.com).

Digital Object Identifier 10.1109/LAWP.2022.3232814

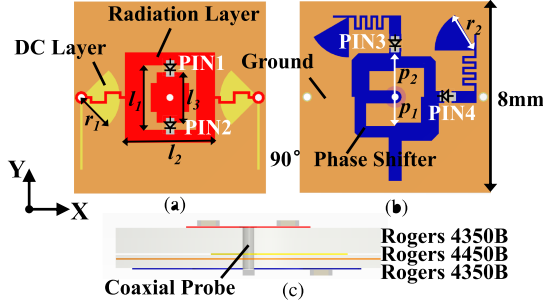


Fig. 1. Geometry of the proposed 2-bit element: (a) top view, (b) bottom view, and (c) side view.

TABLE II
ANTENNA STATUS DEFINED BY DIFFERENT CODES OF P-I-N DIODES

Antenna Mode	PIN1–PIN4	Phase
state 1	1000	0°
state 2	0111	90°
state 3	0100	180°
state 4	1011	270°

substrates are $h_1 = 0.762$ mm and $h_2 = 0.254$ mm. A Rogers 4450F prepreg ($\epsilon_r = 3.5$, $\tan\sigma = 0.002$) with a thickness of 0.101 mm is added between two substrate layers. Different colors distinguish the four-layer metal structure, representing the radiation layer, the dc layer, the ground, and the 90° phase shifter layer, respectively.

The radiation layer is designed based on the square-ring patch with a central metallic strip concept. A coaxial probe is connected to the central metallic strip, and then, two p-i-n diodes (MACOM MA4GP907) are integrated to achieve 180° rotational symmetry structure. As a result, natural 1-bit ($0^\circ/180^\circ$) phase shift can be realized, where the phase states will be dynamically switched with the dc biasing current. The biasing circuit is an important part for switching the p-i-n diodes. In the second layer, a practical biasing structure, which is composed by the bent high-impedance line and radial stub, is used to prevent the RF signal entering the bias line. A cascaded 90° phase shifter is adopted for 2-bit design next. The proposed phase shifter consists of a 3 dB branch-line coupler, two p-i-n diodes, reflective loads, and corresponding dc bias circuits. For the reflection type phase shifter, the perturbed phase is often determined by the reflective loads, which consist of an open-ended transmission line section with adjustable electrical length. The equivalent length will alter depending on whether the switches are turned “ON” or “OFF,” resulting in a 90° phase tuning range.

Table II lists the cascaded 2-bit phase states for different switching modes, where “0” is the reverse-biased mode and “1” is the forward-biased mode. Especially, if the phase of state 1 is selected as reference, when PIN1 and PIN2 are alternatively turned “ON” or “OFF,” the surface currents will be inverted in state 3, i.e., there is a 180° phase difference in states 1 and 3. By activating the diodes of PIN3 and PIN4, an extra 90° phase shift is introduced in states 2 and 4. Hence, a 2-bit phase resolution can be obtained, yielding four distinct phase states.

B. Series-Parallel-Fed 9×8 Array

Based on the proposed reconfigurable 2-bit element, a beam-steerable phased array antenna consisting of 9×8 elements is

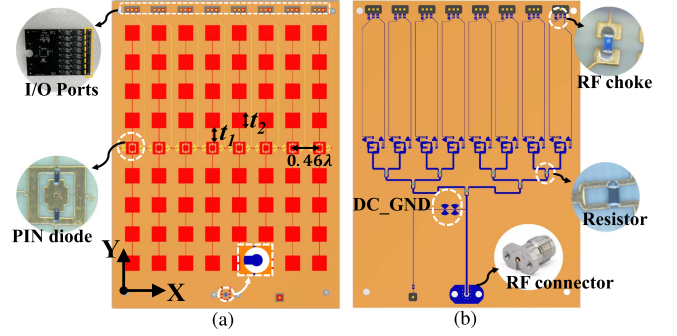


Fig. 2. Geometry of the proposed 9×8 array: (a) top view and (b) bottom view.

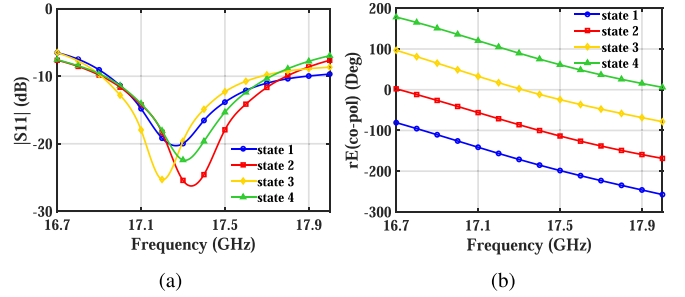


Fig. 3. (a) Simulated reflection coefficients and (b) phase of far-field E-field for the series-fed subarray with different modes.

constructed, as shown in Fig. 2. This array includes eight series-fed linear subarrays, a parallel-fed Wilkinson power divider, and corresponding dc-vias for inserting the control circuit board. The driven 2-bit element and the subarray elements are connected along y -direction (E-plane). To keep the upper and lower parts of the series-fed subarray in phase, an additional 180° phase shift needs to be introduced with a 180° -long transmission line (t_1) [15]. As shown in Fig. 2(a), feed lines are connected in the middle of the radiating edges, then the series-fed subarray is driven by the central element. As shown in Fig. 2(b), a well-known parallel-fed Wilkinson feeding network is used to ensure proper power distribution across all linear subarrays, and then, a common dc ground is integrated in the power divider to form a complete dc loop. A vertical solderless connector is selected for RF signal input. At the same time, a hole is placed in the ground to improve the capacitive mismatch between the RF connector and microstrip line.

The dimension values of the driven element and the parasitic patch are optimized by full-wave simulation software based on the abovementioned analysis. In simulations, the p-i-n diode is modeled as a series of lumped RLC elements: $R_p = 5.8 \Omega$ and $L_p = 30$ pH for “1” state and $C_p = 25$ fF and $L_p = 30$ pH for “0” status. Final dimension values are: $l_1 = 2.7$ mm, $l_2 = 3.74$ mm, $l_3 = 2.1$ mm, $p_1 = 1.21$ mm, $p_2 = 1.8$ mm, $r_1 = 1.6$ mm, $r_2 = 1.65$ mm, $t_1 = 4.13$ mm, and $t_2 = 4.6$ mm. Further simulation in Fig. 3(a) shows the simulated reflection coefficient of the subarray when the diodes are operating in different states. Fig. 3(b) presents the phase of copolarization E-field. Thanks to the 2-bit phase change of the driven element, it can be seen that the phase of the subarray has a 90° difference for four states. The reflection coefficients of all states are less than -10 dB in the frequency band of 16.9–17.7 GHz, and the phase

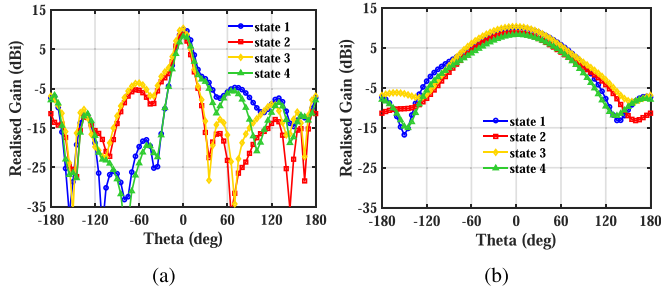


Fig. 4. Simulated radiation pattern of the series-fed subarray with different modes in (a) E-plane and (b) H-plane at 17.3 GHz.

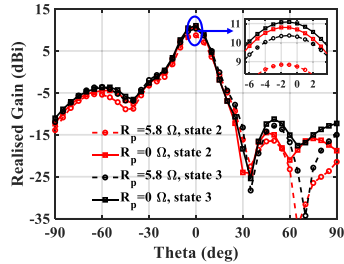


Fig. 5. Effect of the ON-resistance of the p-i-n diode to the gain of subarray.

difference remains 90° within the operating band. The radiation patterns of a linear subarray at 17.3 GHz are shown in Fig. 4. The half-power beamwidth (HPBW) of E-plane (yo -plane) is significantly narrower than that of H-plane (xo -plane), whereas the H-plane radiation pattern matches a single element's exactly. The beamwidth of main lobe in E-plane is about 60° , but it is also noted that the pattern is not symmetric, which may be explained by the asymmetry of the element. At the same time, the currents on the parasitic patch of states 1 and 3 (or states 2 and 4) are opposite because of the reverse states in PIN1 and PIN2, causing their E-plane patterns to be symmetric to each other. Further results show that the peak gains are about 10.4 dBi for states 1 and 3, and about 8.9 dBi for states 2 and 4. It can be found that the difference is about 1.5 dB. This mainly comes from the ON-resistance of the p-i-n diode. As shown in Table II, states 2 and 4 have three diodes be activated, whereas states 1 and 3 only have one diode be activated. However, the insertion loss becomes nonnegligible at Ku -band or higher frequencies. The effect of the ON-resistance of the p-i-n diode to the gain of subarray is shown in Fig. 5. If the equivalent resistor R_p is set to zero, the peak gains of states 2 and 3 are 10.7 and 11 dBi. Therefore, the difference between two states is reduced to 0.3 dB, and the insertion loss caused by the lumped resistor can be calculated to be approximately 2 dB.

III. EXPERIMENTAL RESULTS AND DISCUSSION

The reconfigurable 2-bit subarray in the abovementioned section is used to construct a prototype, as shown in Fig. 6. In total, eight linear subarrays are printed with a space of $0.46\lambda_0$, where λ_0 is the free-space wavelength at 17.3 GHz. This 9×8 array has overall dimension of $92 \text{ mm} \times 68 \text{ mm}$, equivalent to $5.3\lambda_0 \times 3.9\lambda_0$. The antenna array, metal backboard, and control board are fixed by copper cylinders. A commercial ST microcontroller (STM32F103RET6) is adopted to output the “0/1” states of p-i-n diodes. The dc forward-bias voltage is set

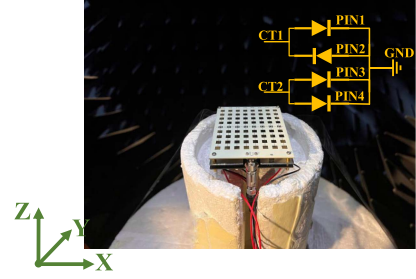


Fig. 6. Photograph of the fabricated reconfigurable 2-bit antenna array in the SATIMO anechoic chamber.

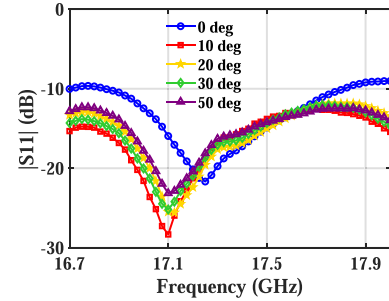


Fig. 7. Measured reflection coefficients for the 9×8 array with different beam directions.

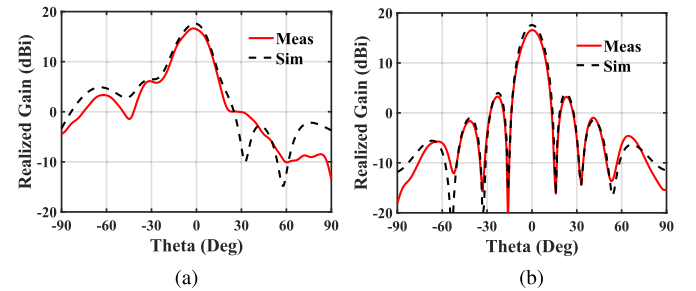


Fig. 8. Simulated and measured radiation pattern of the 9×8 linear array for broadside beam at (a) E-plane and (b) H-plane.

to 3.3 V, and the reverse-bias voltage is set to -3.3 V. There are totally four diodes on each antenna: 1) PIN1 and PIN2 cannot work at the same time, so they must be connected in parallel in opposite directions; 2) PIN3 and PIN4 work at the same state, so they can be multiplexed with the same control port. Thus, a total of $8 \times 2 = 16$ independent I/O ports are provided by the microcontroller.

The measured reflection coefficients of the array are shown in Fig. 7. When all elements are activated, the common operating frequency range of all scanning beam covers from 16.8 to 17.8 GHz. The simulated and measured radiation patterns for broadside beam on E- and H-planes at 17.3 GHz are shown in Fig. 8. In this case, good agreements are found between measurements and simulations in both planes, particularly for the main lobes. The simulated and measured peak gains are 17.6 and 16.6 dBi, respectively. Although some differences are observed in the gain level due to the soldering, fabrication, and assembling errors that are not in to account in the simulations, the HPBW, nulls, and sidelobe level (SLL) are coincided well with the simulated one. It is also noted that the radiation pattern in E-plane

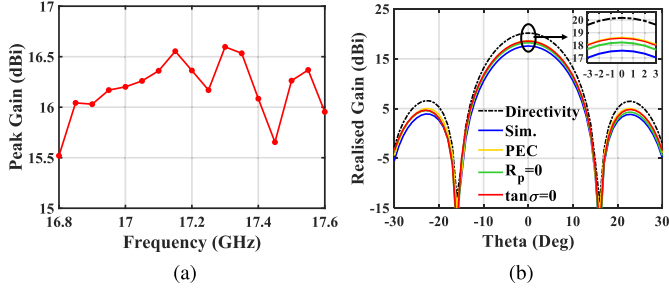


Fig. 9. (a) Measured peak gain of broadside beam and (b) loss analysis on the array gain at 17.3 GHz.

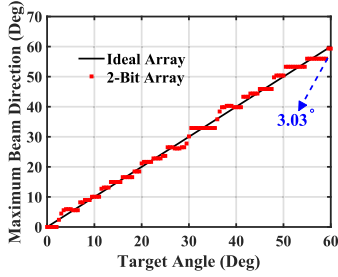


Fig. 10. Maximum beam directions of an eight-element array factor using the continuous phase and 2-bit quantized phase.

is similar to curves in Fig. 4(a) but with gain enhancement. The 1.1 dB gain drop bandwidth of the array spans from 16.8 to 17.6 GHz, as shown in Fig. 9(a). In addition, Fig. 9(b) analyzes the main loss components independently, such as free of resistance loss ($R_p = 0$), free of metal loss (PEC), and free of dielectric loss ($\tan\sigma = 0$). These losses are about 0.7, 1, and 1 dB, respectively. So the total loss is about 2.7 dB.

With adjustable dc control signals, the proposed phased array can scan its beam within the regions of $\pm 50^\circ$. Due to the symmetry, the scanning performance of 0° to -50° is not discussed here for brevity. The calculation method for the 2-bit quantized phase was presented in [13]. Due to the effect of quantization phase error, there is a slight pointing error in the steerable beams. Fig. 10 shows the maximum beam direction of an eight-element linear array using the ideal continuous phase and 2-bit quantized phase from the perspective of the array factor. The target angle is from 0° to 60° with a step of 0.5° . It can be found that the beam pointing error is randomly distributed and can be positive or negative. Within the target angle range, the maximum pointing error is about 3° .

Based on the abovementioned analysis, the simulated and measured steerable radiation patterns of 10° , 20° , 30° , and 50° on the H-plane are shown in Fig. 11. To investigate the insertion losses introduced by the p-i-n diodes at a specified beam angle, we introduce a case where $R_p = 0$ as a comparison. It can be found that the insertion losses are 1.9, 1.4, 1.6, and 1.1 dB, respectively. The measured realized gain for each beam is 14.0, 14.4, 14.3, and 11.9 dBi, respectively, and the corresponding maximum beam pointing is 11° , 21° , 33° , and 50° , respectively. The gain is reduced by around 5 dB when the beam is scanned to 50° , this is mainly caused by the following reasons: first, the pattern of series-fed subarray has a gain decrease of about 3.5 dB at this angle, as shown in Fig. 4(b); second, there is no quantization gain loss for broadside beam, while 1 dB quantization gain loss appears when the 2-bit array scans; third,

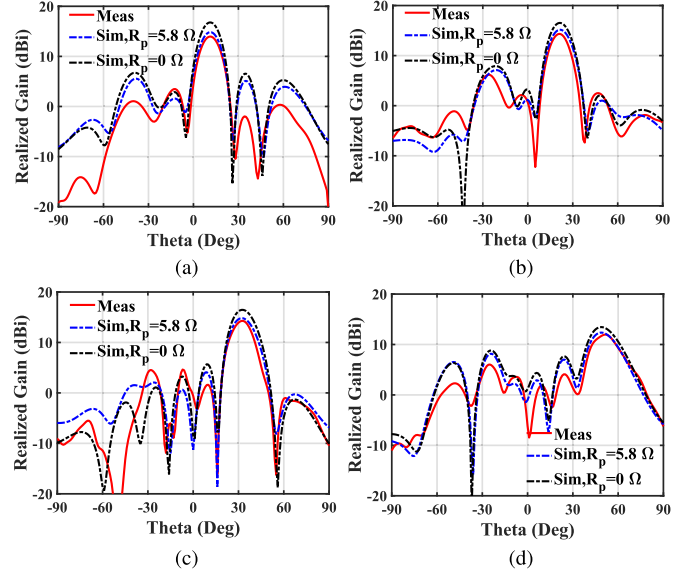


Fig. 11. Simulated and measured radiation pattern of the 9×8 linear array with the cases of 10° , 20° , 30° , and 50° scanning angle. The observation plane is the xoz -plane.

TABLE III
PERFORMANCE INDEXES OF SCANNED BEAMS

Target Angle	Gain (dBi)		SLL (dB)		Scan Angle	
	Sim.	Meas.	Sim.	Meas.	Sim.	Meas.
0°	17.6	16.6	-13.6	-13.3	0°	0°
10°	14.85	14.0	-9.3	-10.5	11°	11°
20°	15.2	14.4	-8.1	-8.3	22°	21°
30°	14.8	14.3	-10.8	-9.6	32°	33°
50°	12.4	11.9	-4.2	-5.8	49°	50°

the insertion loss introduced by the p-i-n diodes is different, where 0.7 dB for broadside beam and 1.1 dB for 50° scanning beam. As the scan angle increases, a relatively high-peak SLL occurs due to the effect of quantization error, which results in increased gain fluctuation. The corresponding performance indexes at 17.3 GHz are summarized in Table III, including the peak gains, SLLs, and actual scan angles. At the expense of slight gain losses and pointing errors, the 2-bit phased arrays are still a cost-effective replacement method compared with continuous scan arrays.

IV. CONCLUSION

In this letter, a series-parallel-fed 2-bit phase array antenna in Ku -band is designed, analyzed, and measured. By switching the “0” and “1” states of p-i-n diodes, a cascaded 2-bit phase shifter can be achieved in the antenna element. Using this 2-bit element as a phase shifter, a series-fed linear subarray is constructed and the simulated results are carried out to verify the production of different phases. A 9×8 array prototype is finally fabricated to demonstrate the flexible beam scanning capability within the scan range of $\pm 50^\circ$ in H-plane. With the advantages of low cost, compact size (0.46λ), and simple phase shifting method, the proposed array is suitable for a variety of wireless communication applications that require beam scanning.

REFERENCES

- [1] C. Liaskos, S. Nie, A. Tsioliaridou, A. Pitsillides, S. Ioannidis, and I. Akyildiz, "Realizing wireless communication through software-defined hypersurface environments," in *Proc. IEEE 19th Int. Symp. A World Wireless, Mobile Multimedia Netw.*, 2018, pp. 14–15.
- [2] M. Renzo et al., "Smart radio environments empowered by ai reconfigurable meta-surfaces: An idea whose time has come," *EURASIP J. Wireless Commun. Netw.*, vol. 2019, no. 1, 2019, Art. no. 129.
- [3] T. N. Le, A. Pegatoquet, T. Le Huy, L. Lizzi, and F. Ferrero, "Improving energy efficiency of mobile WSN using reconfigurable directional antennas," *IEEE Commun. Lett.*, vol. 20, no. 6, pp. 1243–1246, Jun. 2016.
- [4] S. Ciccina, G. Giordanengo, and G. Vecchi, "Energy efficiency in IoT networks: Integration of reconfigurable antennas in ultra low-power radio platforms based on system-on-chip," *IEEE Internet Things J.*, vol. 6, no. 4, pp. 6800–6810, Aug. 2019.
- [5] X. Pan, F. Yang, S. Xu, and M. Li, "A 10 240-element reconfigurable reflectarray with fast steerable monopulse patterns," *IEEE Trans. Antennas Propag.*, vol. 69, no. 1, pp. 173–181, Jan. 2021.
- [6] Y. Xiao, B. Xi, M. Xiang, F. Yang, and Z. Chen, "1-bit wideband reconfigurable transmitarray unit cell based on PIN diodes in Ku-band," *IEEE Antennas Wireless Propag. Lett.*, vol. 20, no. 10, pp. 1908–1912, Oct. 2021.
- [7] J. Hu, Y. Li, and Z. Zhang, "A novel reconfigurable miniaturized phase shifter for 2-D beam steering 2-bit array applications," *IEEE Microw. Wireless Compon. Lett.*, vol. 31, no. 4, pp. 381–384, Apr. 2021.
- [8] P. Liu, Y. Li, and Z. Zhang, "Circularly polarized 2 bit reconfigurable beam-steering antenna array," *IEEE Trans. Antennas Propag.*, vol. 68, no. 3, pp. 2416–2421, Mar. 2020.
- [9] P. Loghmannia, M. Kamyab, M. R. Nikkhah, and R. Rezaiesarlak, "Miniaturized low-cost phased-array antenna using SIW slot elements," *IEEE Antennas Wireless Propag. Lett.*, vol. 11, pp. 1434–1437, 2012.
- [10] L. Chang, Y. Li, Z. Zhang, and Z. Feng, "Reconfigurable 2-bit fixed-frequency beam steering array based on microstrip line," *IEEE Trans. Antennas Propag.*, vol. 66, no. 2, pp. 683–691, Feb. 2018.
- [11] X. Cao, C. Deng, and K. Sarabandi, "Fixed-frequency beam steering leaky-wave antenna with integrated 2-bit phase shifters," *IEEE Trans. Antennas Propag.*, vol. 70, no. 11, pp. 11246–11251, Nov. 2022.
- [12] Y. Wang, F. Xu, Y.-Q. Jin, and Z. Du, "Low-cost reconfigurable 1 bit millimeter-wave array antenna for mobile terminals," *IEEE Trans. Antennas Propag.*, vol. 70, no. 6, pp. 4507–4517, Jun. 2022.
- [13] L. Yin, P. Yang, Y. Gan, F. Yang, S. Yang, and Z. Nie, "A low cost, low in-band RCS microstrip phased-array antenna with integrated 2-bit phase shifter," *IEEE Trans. Antennas Propag.*, vol. 69, no. 8, pp. 4517–4526, Aug. 2021.
- [14] J. Hu and Z.-C. Hao, "A compact polarization-reconfigurable and 2-D beam-switchable antenna using the spatial phase shift technique," *IEEE Trans. Antennas Propag.*, vol. 66, no. 10, pp. 4986–4995, Oct. 2018.
- [15] K. Wincza, S. Gruszczynski, and J. Borgosz, "Microstrip antenna array with series-fed 'through-element' coupled patches," *Electron. Lett.*, vol. 43, no. 9, pp. 487–489, 2007.